Materials Letters 244 (2019) 27–30

Contents lists available at ScienceDirect

Materials Letters

journal homepage: www.elsevier.com/locate/mlblue

Heterogeneous interface induced formation of balsam pear-like PPy for high performance supercapacitors

Lijia Yang [a], Minjie Shi [a], Jintian Jiang [a], Yongchao Liu [a], Chao Yan [a,*], Hu Liu [b,c], Zhanhu Guo [b]

[a] School of Materials Science and Engineering, Jiangsu University of Science and Technology, Zhenjiang 212003, China
[b] Integrated Composites Laboratory (ICL), University of Tennessee, Knoxville, TN 37934, USA
[c] Key Laboratory of Materials Processing and Mold, Zhengzhou University, Zhengzhou 450002, China

ARTICLE INFO

Article history:
Received 13 December 2018
Received in revised form 10 February 2019
Accepted 11 February 2019
Available online 18 February 2019

Keywords:
Energy storage and conversion
Electrodeposition
Supercapacitor
Biomimetic
Polypyrrole

ABSTRACT

In this work, we have put forward a novel heterogeneous interface induced formation strategy to prepare balsam pear-like polypyrrole (PPy) film by using binary electrodeposition. The as-prepared PPy film exhibited a balsam pear-like structure with plenty of vertically aligned serrations and offered a longer conjugation length of PPy chains. Beneficial from the reasonable structure, the serrated PPy (SE-PPy) provided abundant electro-active contact area with the electrolyte, thus leading to the ultrafast-spreading of electrolyte ions and high utilization efficiency of active electrode. Based on this, the SE-PPy electrode showed outstanding electrochemical performance with a large specific capacitance of 773.6 F/g at 1 A/g in 1 M KOH electrolyte, and still retains ~77.6% of its initial capacitance at a high current density of 20 A/g, which is superior to the reported PPy and most of PPy-related electrodes.

1. Introduction

Polypyrrole (PPy) has received much attention due to its high conductivity, reversible doping/dedoping electrochemistry, and low cost [1]. The synthesis strategies of PPy are mainly chemical oxidation and electrochemical deposition [2]. The products obtained by traditional one phase electrochemical deposition are usually aggregated spherical films. However, the aggregated structure of PPy films impedes the ion diffusion into the inner active material, leading to a decreased capacitance. To overcome the obstacles, special PPy structures (such as nanotube, nanoscale and nanowire, etc.) have been prepared to reduce the charge/ion transfer routes [3].

Balsam pear has serrated protrusions on the surface, which greatly enlarge its specific surface area and provide a shorter nutritional transport path. Accordingly, the balsam pear with bulges can transport and store more nutrients compared with that with flat surface. Herein, we reported a novel heterogeneous interface induced formation strategy to prepare balsam pear-like PPy film, which was constructed by plenty of serrated protrusions on the surface. The polymerization occurs at aqueous/organic heterogeneous interface, and the interfacial electro-polymerization is few reported in conducting polymers. The PPy film grown on nickel foam (NF) by a facile binary electrodeposition can be used as a binder-free electrode. Beneficial from the reasonable structure, the SE-PPy electrode can provide abundant electro-active contact area with the electrolyte, thus leading to the ultrafast-spreading of electrolyte ions and high utilization efficiency of active electrode (Fig. 1).

2. Experimental

The schematic illustration of the synthesis of PPy film is shown in Fig. 2a. The NF was ultrasonically washed with acetone, ethanol and deionized (DI) water, respectively, and dried. 40 mL of pyrrole dichloromethane solution (0.1 M) and 40 mL of H_2SO_4 aqueous solution (0.1 M) were transferred to an electrolytic cell successively, where a liquid/liquid two-phase interface formed. Subsequently, the NF used as a working electrode was inserted into the down liquid. The Pt counter electrode and Hg/Hg_2SO_4 reference electrode were inserted into the upper liquid. The PPy film was electrodeposited on the upper part of NF in a three-electrode system under the constant potential of 0.8 V for 300 s. The as-prepared SE-PPy film was washed with DI water and ethanol for several times, and dried at 60 °C for 8 h. As control, the spherical PPy (SP-PPy) was prepared under the same conditions, except the electrolyte was replaced by one phase of 0.1 M pyrrole and 0.1 M H_2SO_4 aqueous solution.

* Corresponding author.
E-mail address: chaoyan@just.edu.cn (C. Yan).

https://doi.org/10.1016/j.matlet.2019.02.064
0167-577X/

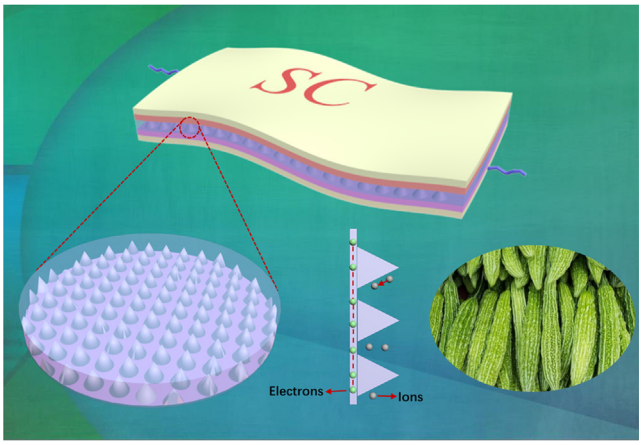

Fig. 1. The electron transfer and ion diffusion pathway on SE-PPy.

The samples were characterized by SEM (ZEISS Merlin Compact), Raman (InVia, Renishaw), FTIR (FTS2000) and XRD (XRD-6000). The electrochemical measurements were carried out in 1 M KOH with a three-electrode system, where Pt and Hg/HgO was served as the counter and reference electrode, respectively.

3. Results and discussion

As schematically illustrated in Fig. 2a, the synthesis process of PPy took place at the heterogeneous interface between the dilute sulfuric acid solution and pyrrole/dichloromethane solution, and then PPy grew on the upper side of NF in the dilute sulfuric acid solution. However, the PPy grew on the whole surface of NF in a one-phase system. The morphology of PPy films was explored by SEM (Fig. 2(b and c)). As observed, SE-PPy presents plenty of serrated protrusions, just like the surface structure of balsam pear. The surface protrusions of SE-PPy can furnish a larger contact area between the electrolyte and the electrode, and thus effectively boost the accessible active sites for electrolyte ions and electrons. By contrast, the SP-PPy was spherical and relatively flat.

The Raman spectra of both samples (Fig. 2d) presented the characteristic Raman shifts of PPy, such as 1590, 1495, 1405, 1330, 1044, 982 and 927 cm^{-1} [4]. It was reported the intensity ratio of the C = C stretching mode at 1590 cm^{-1} (I_{1590}) and the skeletal band at 1495 cm^{-1} (I_{1495}) can reflect the conjugation length of PPy chains [5], and the conjugation length increases with the increase of the I_{1590}/I_{1495}. The I_{1590}/I_{1495} of SE-PPy (1.9) is higher than that of SP-PPy (1.6), indicating a longer conjugation length of SE-PPy. The longer conjugation length can offer a higher conductivity and faster charge transport rate of SE-PPy.

Fig. 2e shows the FTIR spectra of SE-PPy and SP-PPy. The characteristic peaks of PPy are presented at 1465, 1553, 1633, 1050, 901 and 780 cm^{-1}.[6] The conjugation length of PPy can be evaluated by the ratio of integrated absorption area of the asymmetric ring stretching (A_{as1553}) to the symmetric stretching (A_{s1465}) [6]. And the conjugation length increases with the decrease of A_{as1553}/A_{s1465}. Compared with SP-PPy (7.06), a lower A_{as1553}/A_{s1465} value of SE-PPy (4.09) indicates a longer conjugation length, which is consistent with the Raman result. As shown in Fig. 2f, there are three strong XRD diffraction peaks at 44.2°, 51.6°, 76.1°, which were indexed to (1 1 1), (2 0 0) and (2 2 0) planes of NF, respectively. Both PPy samples are amorphous as indicated by the broad peak located at around 23° (inset of Fig. 2f).

Fig. 3a shows the CV curves of SE-PPy and SP-PPy at a scan rate of 50 mV/s. A pair of redox peaks on the CV curves indicates that

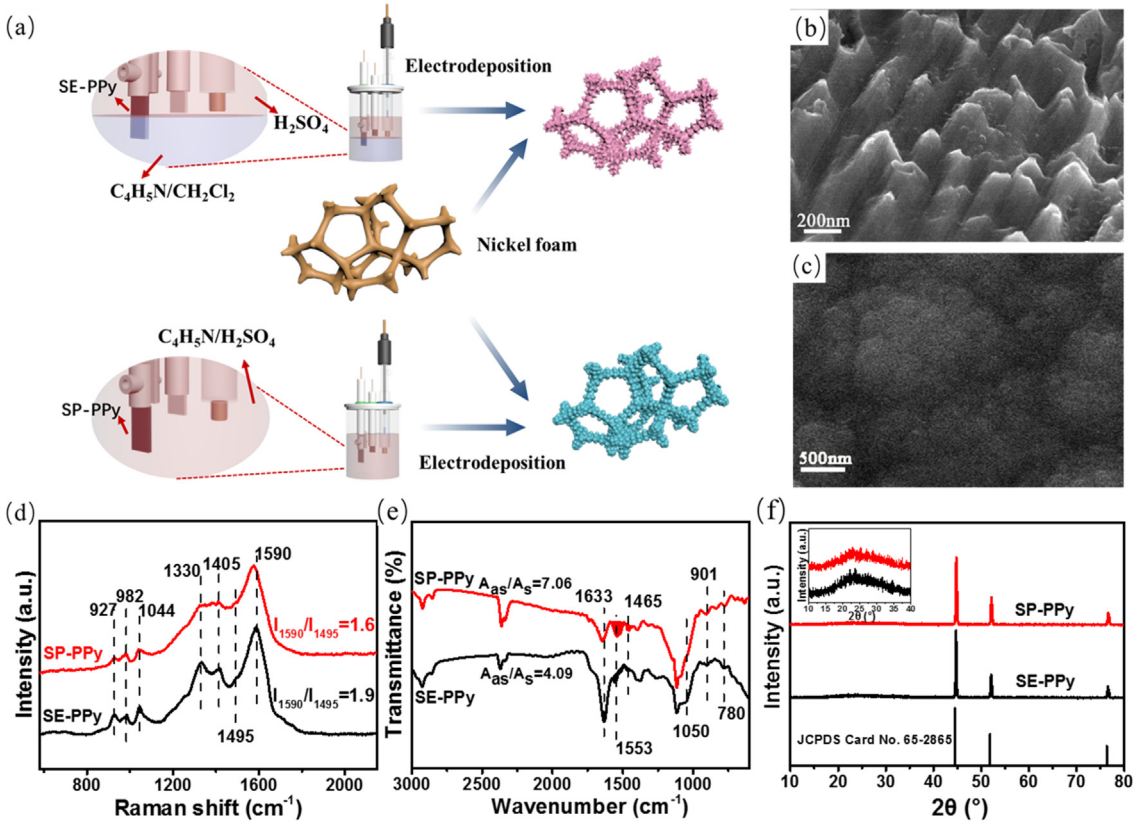

Fig. 2. (a) Schematic illustration of the electrochemical deposition of PPy film on NF; SEM images of (b) SE-PPy, (c) SP-PPy; (d) Raman spectra, (e) FTIR spectra and (f) XRD patterns of SE-PPy and SP-PPy.

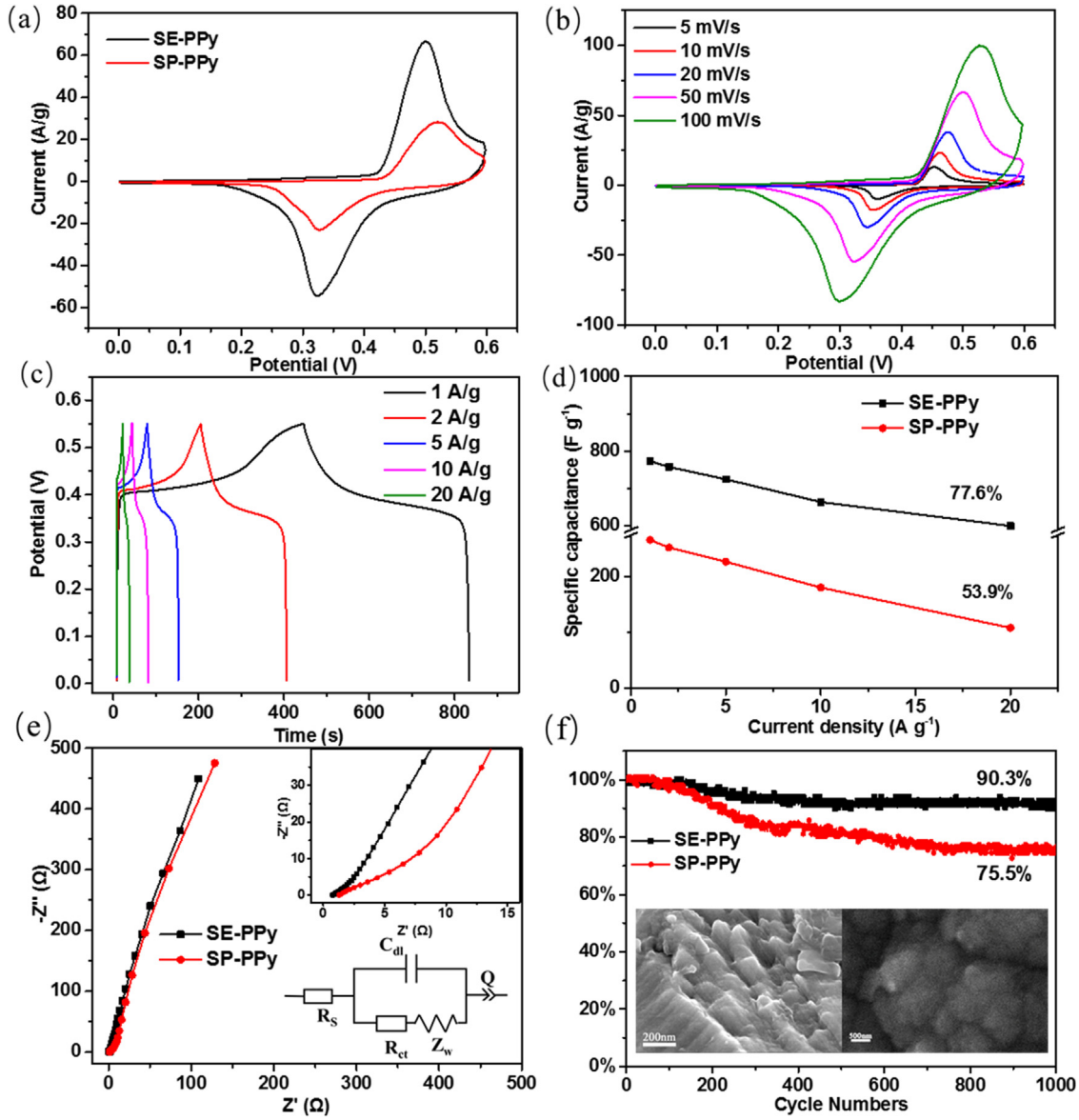

Fig. 3. (a) CV curves of SE-PPy, SP-PPy at 50 mV/s; (b) CV curves of SE-PPy at different scan rates; (c) GCD curves of SE-PPy at various current densities; (d) Specific capacitance at different current densities. (e) EIS plots of SE-PPy and SP-PPy; (f) cycling stability at 5 A/g, the insert is SEMs of SE-PPy and SP-PPy after 1000 cycles.

the energy storage of polypyrrole electrodes follows the pseudopotential mechanism. Compared with SP-PPy, the integral area of the CV curve of SE-PPy is apparently larger than that of SP-PPy, which reveals the superior capacitance of SE-PPy. With increasing the scan rate, the oxidation and reduction peak shifts toward to higher and lower potential (Fig. 3b), respectively, which may be ascribed to the polarization effect of the electrode. Moreover, no distinct distortion can be observed on CV curves with increasing the sweep rate, suggesting a low resistance and good reversible property of the SE-PPy. The electrochemical kinetics of electrodes can be described by the relationship of peak current (i) and scan rate (v): $i = av^b$. The calculated b-value (the adjacent value) of SE-PPy for the anodic and cathodic peak currents is 0.67 and 0.71, respectively, suggesting that the process is not only controlled by the capacitance effect, but also determined by the diffusion.

The nearly symmetric GCD profiles of SE-PPy at different current densities are shown in Fig. 3c. The obviously observed pair of platforms in the GCD curves correspond to the redox processes of the CV curves. The SE-PPy exhibits the highest specific capacitance (Cs) value of 773 F/g, which is much higher than that of SP-PPy (266.4 F/g). With the current density increased from 1 to 20 A/g, the Cs of the SE-PPy maintained at about 77.6%, which is much better than that of SP-PPy (53.9%) (Fig. 3d). The electrochemical impedance spectroscopy (EIS) test was employed in the frequency range from 100 kHz to 0.01 Hz as shown in Fig. 3e. In the low frequency region, the straight line parts of SE-PPy is more parallel to the imaginary axis than that of SP-PPy, suggesting its better capacitive response [7]. The Nyquist plot of SE-PPy and SP-PPy can be well fitted to an equivalent circuit consisting of R_s (equivalent series resistance), C_{dl} (double-layer capacitance), R_{ct} (charge transfer resistance), Z_W (Warburg-type resistance) and Q (pseudocapacitance) (inset of Fig. 3e). The intercepts with the x-axis, used to determine the R_s, are obtained to be 0.763 and 1.276 Ω for SE-PPy and SP-PPy, respectively. The cycling performance of SE-PPy showed the capacitance retention of 90.3% after 1000 cycles at 5 A/g, superior to that of SP-PPy (75.5%) (Fig. 3f). In addition, the morphology of SE-PPy and SP-PPy electrodes scarcely changed after 1000 cycles (inset of Fig. 3f).

The outstanding performance of SE-PPy (773.6F/g at 1 A/g) is superior to that of PPy and most of PPy-related electrodes, such as PPy nanoparticles (356 F/g at 10 mV/s) [8], GO/PPy composites (481.1 F/g at 0.77 A/g),[9] PPy/rGO/ZrO_2 composites (341 F/g at 0.5 A/g) [10], and so on (Table S1). This superior electrochemical performance is attributed to the following reasons. The longer conjugation length of SE-PPy introduced by the binary electrodeposition provides a higher conductivity and a faster charge transport rate. And the unique structure supplies much more accessible active sites for electrolyte ions and electrons and improves the utilization efficiency of active electrode.

4. Conclusions

In summary, a novel heterogeneous interface induced formation strategy was reported to prepare balsam pear-like PPy film, which was constructed by plenty of serrated protrusions on the surface. The specific capacitance of SE-PPy at 1 A/g was 773.6 F/g, and the capacitance retention is 90.3% after 1000 cycles at 5 A/g. It maintained ~77.6% when the current density was increased to 20 A/g. Considering the facile fabrication and outstanding performance, this work represents a quantum leap forward in the search of new electrode materials for high performance supercapacitors.

Conflict of interest

The authors declare no competing financial interest.

Declaration of interest

None.

Acknowledgements

We greatly acknowledge the funding from the National Natural Science Foundations of China (51873083), the Opening Project of State Key Laboratory of Polymer Materials Engineering (Sichuan University) (No. sklpme2018-4-27), the Six Talent Peaks Project in Jiangsu Province (No. 2015-XCL-028), the Postgraduate Research & Practice Innovation Program of Jiangsu Province (KYCX17_1831, SJCX18_0759).

Appendix A. Supplementary data

Supplementary data to this article can be found online at https://doi.org/10.1016/j.matlet.2019.02.064.

References

[1] M. Zhu, Y. Huang, Q. Deng, J. Zhou, Z. Pei, Q. Xue, et al., Adv. Energy Mater. 6 (21) (2016) 1600969.
[2] Y. Huang, H. Li, Z. Wang, M. Zhu, Z. Pei, Q. Xue, et al., Nano Energy 22 (2016) 422–438.
[3] Y. Zheng, J. Xu, X. Yang, Y. Zhang, Y. Shang, X. Hu, Chem. Eng. J. 333 (2018) 111–121.
[4] H. Yao, F. Zhang, G. Zhang, H. Luo, L. Liu, M. Shen, et al., Chem. Eng. J. 334 (2018) 2547–2557.
[5] S. Demoustier-Champagne, P.-Y. Stavaux, Chem. Mater. 11 (1999) 829–834.
[6] N. Bai, Z. Xu, Y. Tian, L. Gai, H. Jiang, K. Marcus, et al., Electrochim. Acta. 249 (2017) 360–368.
[7] Z. Wang, D.O. Carlsson, P. Tammela, K. Hua, P. Zhang, L. Nyholm, et al., ACS Nano 9 (7) (2015) 7563–7571.
[8] S. Chen, H. Liu, Y. Wang, S. Xu, W. Liu, D. He, et al., Electrochimica Acta. 232 (2017) 72–79.
[9] J. Cao, Y. Wang, J. Chen, X. Li, F.C. Walsh, J.-H. Ouyang, et al., J. Mater. Chem. A 3 (27) (2015) 14445–14457.
[10] A.P.P. Alves, R. Koizumi, A. Samanta, L.D. Machado, A.K. Singh, D.S. Galvao, et al., Nano Energy 31 (2017) 225–232.